

Structure of the Water Channel AqpZ from *Escherichia coli* Revealed by Electron Crystallography

P. Ringler¹, M. J. Borgnia², H. Stahlberg¹, P. C. Maloney³, P. Agre²
 and A. Engel^{1*}

¹*M.E. Müller Institute for Microscopy, Biozentrum University of Basel Klingelbergstrasse 70 CH-4056, Basel, Switzerland*

²*Department of Biological Chemistry, Johns Hopkins University School of Medicine Baltimore, MD 21205, USA*

³*Department of Physiology Johns Hopkins University School of Medicine, Baltimore MD 21205, USA*

Molecular water channels (aquaporins) allow living cells to adapt to osmotic variations by rapid and specific diffusion of water molecules. Aquaporins are present in animals, plants, algae, fungi and bacteria. Here we present an electron microscopic analysis of the most ancient water channel described so far: the aquaporin Z (AqpZ) of *Escherichia coli*. A recombinant AqpZ with a poly(histidine) tag at the N terminus has been constructed, overexpressed and purified to homogeneity. Solubilized with octylglucoside, the purified AqpZ remains associated as a homotetramer, and assembles into highly ordered two-dimensional tetragonal crystals with unit cell dimensions $a = b = 95 \text{ \AA}$, $\gamma = 90^\circ$ when reconstituted by dialysis in the presence of lipids. Three-dimensional reconstruction of negatively stained lattices revealed the $p4_2$ packing arrangement that is also observed with the human erythrocyte water channel (AQP1). The 8 \AA projection map of the AqpZ tetramer in frozen hydrated samples is similar to that of AQP1, consistent with the high sequence homology between these proteins.

© 1999 Academic Press

Keywords: aquaporin; major integral protein family; 2D crystallization; electron crystallography; STEM

*Corresponding author

Introduction

As solvent for the chemical processes of life water passes across membranes by diffusion either through the bilayer or through highly specific water pores, the aquaporins. Their presence has been postulated in special membranes exhibiting high osmotic permeability, because the activation energy for the diffusion through the lipid is high (reviewed by Finkelstein, 1987). The discovery of the first aquaporin (AQP1) in the human red cell membrane provided the molecular explanation for selective osmotic water flow across cell membranes (Preston & Agre, 1991). Aquaporins with multiple physiological functions have been reported in mammals and have been shown to be involved in

several clinical disorders (for a review, see King & Agre, 1996). Mammalian aquaporin mutants have been identified with phenotypes including lens cataract (MIP, the major intrinsic protein of lens fiber cells; Shiels & Bassnett, 1996), loss of the red cell Colton blood group antigens (AQP1; Agre *et al.*, 1995), nephrogenic diabetes insipidus (AQP2, the water channel of the collecting duct; Deen *et al.*, 1995), and incomplete renal fluid concentration (AQP4; Verkman *et al.*, 1995). Aquaporins have also been found in frogs (Abrami *et al.*, 1994), insects (Le Cahérec *et al.*, 1996), plants (Weig *et al.*, 1997) and bacteria (Calamita *et al.*, 1995). This widespread occurrence in plant and animal kingdoms suggests an essential physiological function.

Discovery of the *aqpZ* gene in the wild-type *Escherichia coli* was achieved by homology cloning using the sequence-related bacterial gene of the glycerol facilitator (*glpF*). The *aqpZ* DNA from *E. coli* contains a 693 base-pair open reading frame encoding a polypeptide whose sequence is 28–38% identical to those of other known aquaporins (Calamita *et al.*, 1995). Comparative transport analysis using injection of AqpZ cRNA in *Xenopus* oocytes and assays for water or glycerol permeability demonstrated the high water-selectivity

Abbreviations used: AqpZ, aquaporin Z; AQP1, aquaporin 1; 2D, two-dimensional; 3D, three-dimensional; DMPC, 1,2-dimyristoyl-*sn*-glycero-3-phosphocholine; IQ value, measure of the signal-to-noise ratio in diffraction spots; LPR, lipid-to-protein ratios; MIP, major intrinsic protein; MSA, multivariate statistical analysis; OG, octyl- β -D-glucopyranoside; POPC, 1-palmitoyl-2-oleoyl-*sn*-glycero-3-phosphocholine.

E-mail address of the corresponding author: aengel@ubaclu.unibas.ch

and negligible glycerol transport of AqpZ (Calamita *et al.*, 1995). Disruption of the chromosomal *aqpZ* gene is not lethal, but Calamita *et al.* (1988) have shown that AqpZ knockout *E. coli* strains exhibited greatly reduced colony formation at maximum growth rate (39 °C) or when grown at low osmolarity. Those authors propose that the physiological significance of AqpZ for the bacterium is to maintain cell turgor while facilitating volume expansion during cell division.

The amino acid sequence deduced from the *aqpZ* gene possesses the two highly conserved tandem repeats that are present in all members of the aquaporin family. Hydrophathy analysis of this sequence suggests that there are six transmembrane domains consistent with other aquaporins (Calamita *et al.*, 1995; Park & Saier, 1996). Sequence alignment with known aquaporins revealed the presence of highly conserved residues in transmembrane domains as well as the two typical Asn-Pro-Ala (NPA) aquaporin signature motifs located in loops B and E (Calamita *et al.*, 1995) that have been shown to fold back into the membrane (Jung *et al.*, 1994).

The most advanced structure analysis has been performed on AQP1 (Walz *et al.*, 1995, 1997; Japelli, 1995; Li *et al.*, 1997; Cheng *et al.*, 1997). Its three-dimensional structure at 6 Å reveals the predicted six transmembrane spanning alpha-helices and an additional central density that is proposed to contain the extended loops B and E with the highly conserved NPA motifs (Walz *et al.*, 1997). Considerably less is known about the structure of prokaryotic water channels. AqpZ from *E. coli* can therefore be taken as a model system for biophysical investigations, with the advantage of a convenient homologous expression system for mutagenesis.

We report here an electron crystallographic study of this first prokaryotic water channel described. The solubilized AqpZ oligomers are characterized and their two-dimensional crystallization by reconstitution in lipid bilayers is described. Highly ordered 2D crystals were studied by electron crystallography to provide an 8 Å projection map of this prokaryotic aquaporin.

Results

Solubilized AqpZ particles

A construct of AqpZ with an additional 10-histidine tag at the N terminus (molecular mass 26.5 kDa) has been designed, overexpressed in *E. coli*, and milligram amounts of pure and active protein have been isolated by nickel-chelator-based chromatography (Borgnia *et al.*, 1999, accompanying paper). Solubilized AqpZ migrated at a relative molecular mass of 70 kDa in denaturing SDS-polyacrylamide gel electrophoresis (12%), suggesting a tetrameric form (Borgnia *et al.*, 1999).

Micrographs of negatively stained AqpZ particles solubilized in octyl- β -D-glucopyranoside (OG) recorded at a magnification of 70,000 \times

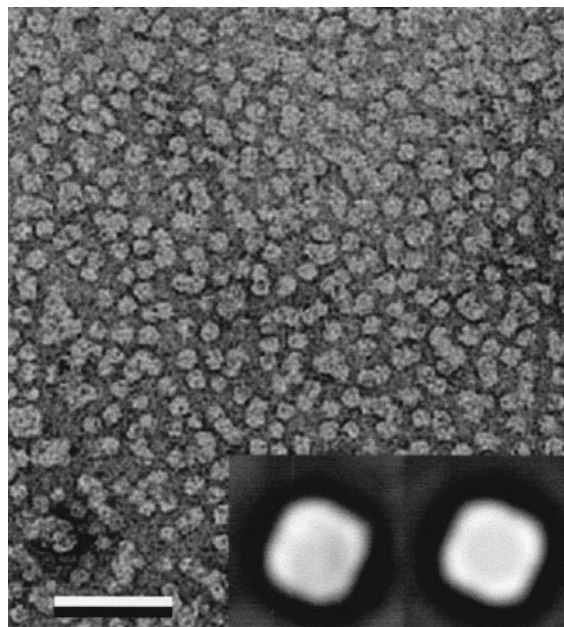


Figure 1. Electron micrograph of negatively stained AqpZ particles solubilized in OG and recorded at 70,000 \times magnification. The particles are rather homogeneous in size and shape. Inset: out of 639 particles, 181 particles with the highest 4-fold symmetry were selected to calculate the final average. It has a clear square-like shape and is shown before (at left) and after 4-fold symmetrization (at right). Scale bar represent 50 nm and the height of the inset is 15 nm.

showed a homogeneous size distribution (Figure 1). The protein particles appeared white on a dark background (negative staining) and many particles exhibited a square shape. To enhance these features, 639 particles were selected by eye on a single micrograph, aligned with respect to a reference and classified into clusters by multivariate statistical analysis (MSA; van Heel & Frank, 1981). An average of 181 aligned particles from five clusters exhibited a square-like shape with 80 Å side length, and showed the tetrameric structure without symmetrization (Figure 1, inset). Although other cluster averages had similar dimensions, they did not show a pronounced 4-fold symmetry, most likely because these tetramers were tilted with respect to the carbon film.

Reconstitution and crystallization

The crystallization procedures were derived from the conditions yielding highly ordered 2D crystals of AQP1 (Walz *et al.*, 1994a) or MIP (Hasler *et al.*, 1998b). Solubilized and purified AqpZ was mixed with various phospholipids in the presence of OG and reconstituted at various lipid-to-protein ratios (LPR, w/w) by dialysis against different buffers (Jap *et al.*, 1992; Hasler *et al.*, 1998a). The crystallization trials were checked for two-dimensional crystals by transmission elec-

tron microscopy of negatively stained samples. Whenever the AqpZ protein was reconstituted into lipid bilayers it exhibited a marked propensity to self-assemble into square arrays. At LPR ~ 2 flattened vesicles were observed with densely packed square particles corresponding to AqpZ tetramers. They were similar to the single particle averages in Figure 1, and self-assembled into mosaic tetragonal lattices (Figure 2(a)).

The main feature observed in a large variety of crystallization conditions was that the 2D crystals of AqpZ had a high propensity to pile-up into three-dimensional stacks (Figure 2(b) and (c)). Some rare side views allowed the thickness of a single layer 2D crystal to be estimated to ~ 61 Å (Figure 2(d)), close to the thickness of AQP1 crystals (58 Å), as measured with the atomic force microscope (AFM; Müller & Engel, 1997). To test whether the stacking was related to the N-terminal poly(histidine), this charged tail was digested with trypsin before crystallization. Under the conditions used, no difference in the crystallization behavior could be detected.

Crystallization was optimized when purified AqpZ protein was mixed in the presence of OG at 0.5 mg/ml final protein concentration with synthetic lipids (POPC and DMPC in the ratio 1:1, w/w) at an LPR between 0.3 and 0.4, and dialyzed against 20 mM citrate buffer (pH 6.0) containing 200 mM NaCl, 100 mM MgCl₂, 3 mM NaN₃ and 10% glycerol. Under these conditions a mixture of μ -sized unilamellar vesicles and single-layered sheets with straight edges assembled, which were all found to have their entire surfaces covered with ordered arrays of the AqpZ oligomer.

Analysis of negatively stained 2D crystals

Transmission electron microscopy of negatively stained vesicles and sheets showed AqpZ 2D crystals with $p4_2$ symmetry (Figure 3) and unit cell dimensions of $a = b = 95.0 \pm 0.1$ Å ($n = 30$). Single-layer 2D crystals exhibited characteristic straight edges with visible steps or cracks along lattice lines (Figure 3(a)). Power spectra of such crystals often showed diffraction spots up to the sixth order in negative stain (Figure 3(a), inset). However, in

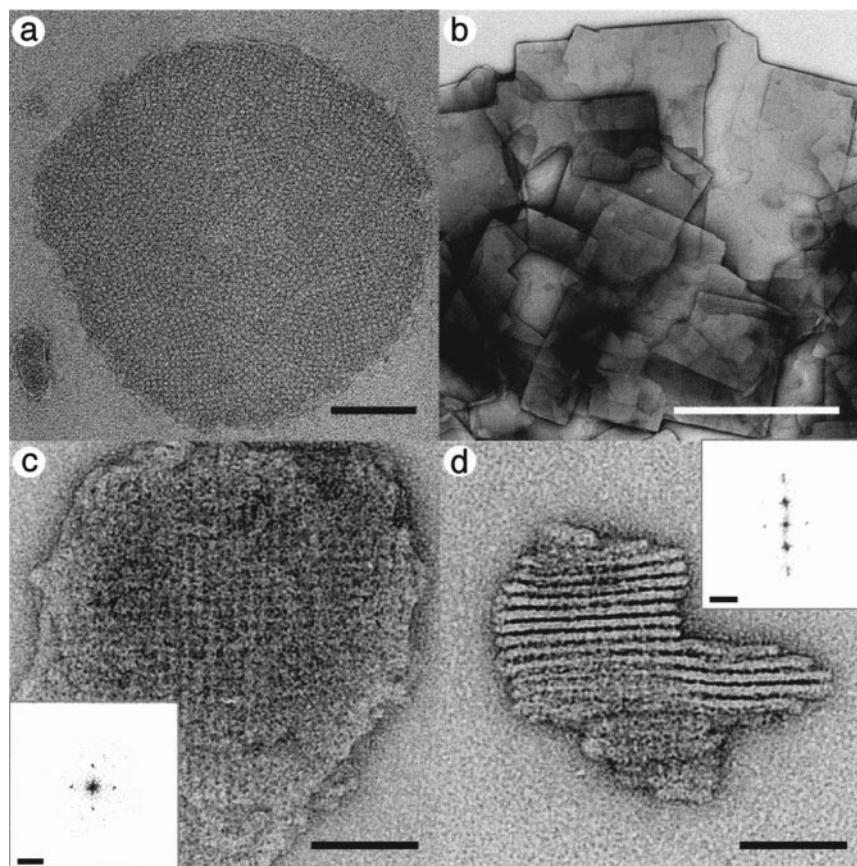


Figure 2. Electron micrographs of negatively stained AqpZ tetramers reconstituted into lipid bilayers. (a) Flattened vesicles with densely packed square-shaped particles corresponding to AqpZ tetramers self-assembled into mosaic tetragonal lattices at a lipid-to-protein ratio of ~ 2 . (b) Large piled-up AqpZ 2D crystal sheets with typical straight edges. (c) Small three-dimensional stack of AqpZ 2D crystals with the corresponding optical diffraction pattern (bottom left). (d) Side view of a 3D stack and the corresponding optical diffraction pattern (top right corner) with a layer spacing of ~ 61 Å. Scale bars represent 100 nm in (a), 1 μ m in (b), 50 nm in (c) and (d), and 5 nm^{-1} in the power spectrum inserts.

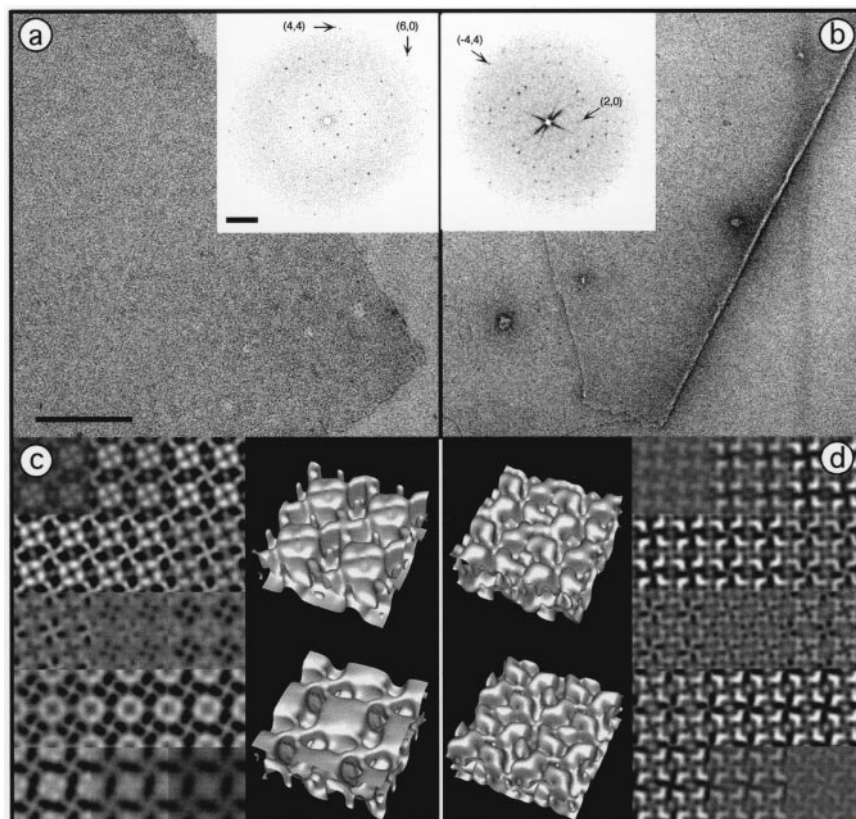


Figure 3. Electron microscopy and image processing of negatively stained AqpZ 2D crystals. (a) A single layer AqpZ 2D crystal. The crystalline sheet has straight edges, and a regular rectangular pattern can be seen when observed at glancing angle. The power spectrum exhibits diffraction spots up to the sixth order (see arrow). The presence of the (1,0) reflection is characteristic for different staining of the crystal. (b) Folded AqpZ 2D crystal sheet. Two sets of diffraction spots are visible, rotated with respect to one another by $\sim 12^\circ$ in the power spectrum. (c) and (d) 3D maps of negatively stained AqpZ 2D crystals calculated from a tilt series comprising 25 projections distributed over -60° to $+60^\circ$. In (c) the left side shows fifteen 3 Å thick, horizontal sections of the single layer crystal (a). The perspective view on the right illustrates the flattening of the surface that was contact with the carbon film. In (d) 15 horizontal sections of one layer of the folded crystal (b) are shown on the right. Both surfaces of this layer are nearly identical, taking the shift of half a unit cell into account, as illustrated by the perspective view on the left. The unit cells house two adjacent tetramers, incorporated in opposite orientations. Horizontal sections in the middle of the membrane show only low contrast because this region is not accessible to the negative stain. Perspective views of the 3D maps were isocontoured at the steepest gradient by a tool kindly provided by Dr B. Heymann. Scale bars represent 300 nm in (a) and 5 nm^{-1} in the diffraction pattern. The side length of the horizontal section is 190 Å.

most cases, power spectra of single-layer 2D crystals had a prominent first diffraction order that is expected to vanish for $p4_21_2$ crystals. Folded sheets (Figure 3(b)) had power spectra showing two distinct sets of diffraction spots rotated with respect to one another by an arbitrary angle. The negative staining of one layer was usually more uniform than that of the other layer as judged from the diffraction pattern of untilted AqpZ 2D crystals. However, the expected systematic absences for $(2n+1,0)$ reflections indicated an appropriate negative staining for both layers (as is demonstrated in Figure 3(b), inset).

To study this in more detail, tilt series were acquired from the two crystals in Figure 3, using automated tomography (Dierksen *et al.*, 1992). The 3D maps are displayed either as horizontal sections of 3 Å thickness (Figure 3(c), left, and 3(d), right) or as surface rendered views (Figure 3(c), right,

and 3(d), left). The 3D map calculated from the negatively stained single layered crystal (Figure 3(c)) is consistent with an up and down packing arrangement of the AqpZ tetramers. Adjacent tetramers expose different surfaces to one side of the layer, one tetramer being bold and the other being thinner, having the shape of a cross. Similar features were seen on the other side of the layer, except that the surface of the bold tetramer shows less detail and is flatter. The flattening is likely to result from the interaction of this tetramer surface with the carbon support, preventing appropriate embedding in the negative stain (Baumeister *et al.*, 1986).

The 3D map obtained from one layer of the negatively stained double-layered crystal also showed two membrane-spanning AqpZ tetramers incorporated in the bilayer with opposite orientation (Figure 3(d)). However, this 2D crystal is

more symmetrically stained, resulting in a map that is very similar at the top and the bottom. The AqpZ tetramer on one surface has a windmill shape with a distinct vorticity, while the other surface exposes a smaller, cross-shaped structure.

Because the aqueous staining solution cannot penetrate into the lipid bilayer, the horizontal sections in the 3D map corresponding to the inner part of the bilayer show only low contrast compared to upper and lower surfaces (Figure 3(c) and (d)); the remaining contrast reflecting the limited resolution along the normal to the membrane plane.

Mass analysis

Scanning transmission electron microscopy (STEM) mass analysis (Müller *et al.*, 1992) of single-layer 2D crystals yielded a mass loss corrected mass/area histogram with one single peak at $3.19(\pm 0.11)$ kDa/nm² (Figure 4). Therefore each unit cell comprising an area of 90.25 nm² has a mass of 288 kDa. Considering two tetramers of AqpZ (eight monomers estimated at 212 kDa total mass according to their amino acid sequence), this unit cell mass allows for 76 kDa of surrounding phospholipids, giving an LPR of 0.35. Taking the value of 717 Da for the mean molecular mass of the POPC/DMPC 1:1 (w/w) lipid mixture used for crystallization, and a packing density of 4 lipids/nm², the interspersed lipid bilayer should cover 30% of the unit cell area (mean value of 106 lipid molecules per unit cell).

Cryo-electron microscopy of unstained AqpZ 2D crystals

Power spectra of micrographs of unstained crystalline patches showed weak diffraction spots up to 8 Å, indicating a significant improvement in resolution compared to negative staining (Figure 5(a)). The six best images (corresponding to ~11,000 unit cells) were unbent, CTF corrected, and an averaged projection map was calculated from the merged amplitudes and phases to a resolution of 8 Å, enforcing the $p4_2$ symmetry (Figure 5(b) and (c)).

The overall shape of the projection of the untilted AqpZ tetramer resembles a four-leafed clover. The monomeric AqpZ is proposed to correspond to one leaf and is formed by seven high-density regions separated by ~8 Å (Figure 5(c)).

Discussion

The first structural analysis of the *Escherichia coli* water channel AqpZ by electron crystallography is presented. Negatively stained OG-solubilized AqpZ preparations revealed a homogeneous particle distribution concerning both size and shape (Figure 1). Previous studies of water channel proteins by freeze-fracture electron microscopy showed tetragonal arrays of the major intrinsic lens protein (MIP; Zampighi *et al.*, 1982), of the insect aquaporin AQPcic (Beuron *et al.*, 1995), and tetramers of the human aquaporin AQP1 (Verbavatz *et al.*, 1993). These are all present in native membranes, suggesting a tetrameric assembly of native water channels. Both MIP and

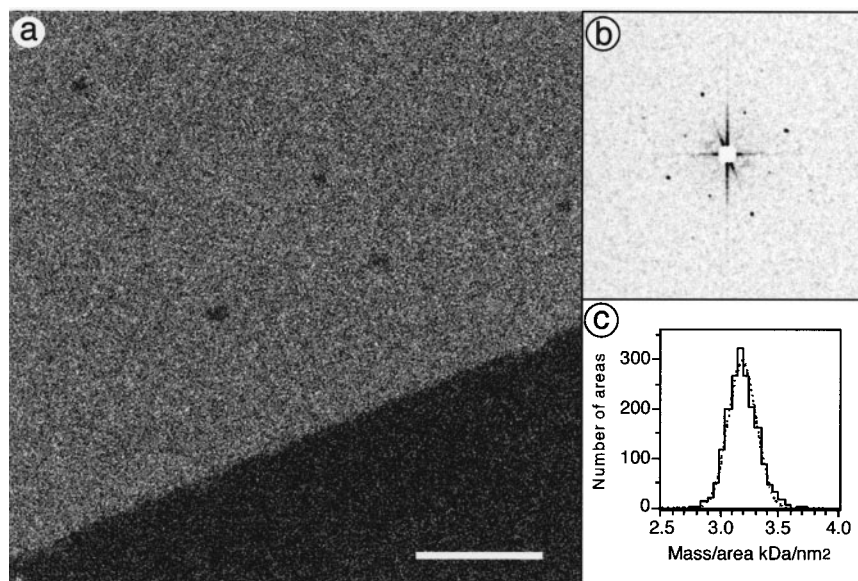


Figure 4. Mass/area measurements of single layer AqpZ 2D crystal using STEM. (a) Elastic dark-field image of an unstained sample recorded at a dose of $330(\pm 23)$ electrons/nm² reveals the typical straight edges of AqpZ single layer 2D crystals and a faint regular pattern. (b) The power spectrum of the dark-field image (a) shows reflections extending to the second order, allowing the unit cell dimensions of the freeze-dried tetragonal lattice to be estimated to $a = b = 95.0(\pm 0.1)$ Å. (c) The mass loss corrected mass/area histogram shows one single peak of $3.19(\pm 0.11)$ kDa/nm², indicating that each unit cell comprising an area of 90.25 nm² has a mass of 288 kDa. Scale bar represents 100 nm in (a).

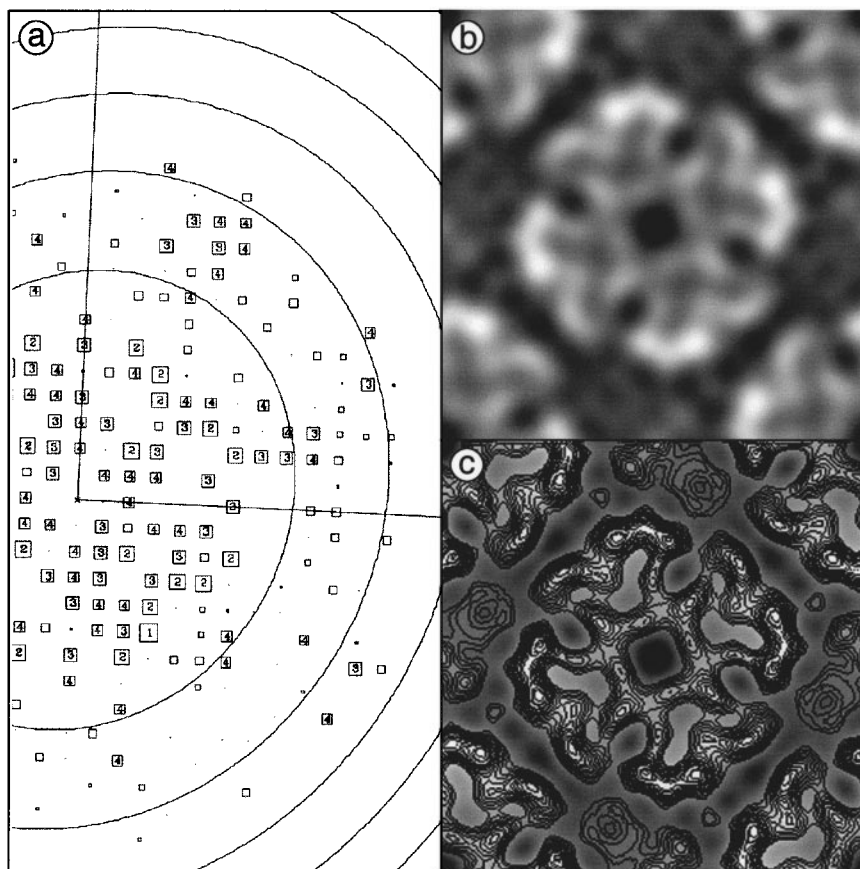


Figure 5. Cryo-EM power spectrum of an untilted AqpZ 2D crystal and the 8 Å projection map. (a) The power spectrum is shown with boxed numbers of the calculated diffraction pattern of one single crystalline area representing the calculated IQ values for the measured diffraction spots as defined by Henderson *et al.* (1986). (b) Averaged projection map calculated to a resolution of 8 Å obtained by merging the data from six highly ordered crystalline areas (with $p4_212$ symmetry imposed). In the displayed unit cell, the central AqpZ tetramer resembles a four-leafed clover, where each leaf is proposed to be the monomeric AqpZ. (c) The projection map from (b) displayed with contour levels showing that the monomer of AqpZ is formed by seven high density regions separated by about 8 Å. The side length of the projection maps (c) and (d) is 95 Å.

AQP1 have been solubilized with OG as tetramers (Smith & Agre, 1991; Walz *et al.*, 1994a; Hasler *et al.*, 1998b). Our finding that solubilized AqpZ remains associated as a tetramer corroborates the idea that the functional oligomer *in vivo* is tetrameric.

Owing to the stability of purified, OG-solubilized AqpZ preparations, the 2D crystallization trials could be performed at room temperature over several days, using dialysis. Tetragonal arrays of AqpZ tetramers were obtained under various conditions, at LPR values between 0.3 and 1, but were often stacked in multilayers (five to ten layers), indicating the possibility of initiating the growth of 3D crystals suitable for X-ray crystallography. Interestingly, the stacking was not affected by the presence or absence of the N-terminal poly(histidine) tail. The use of both a dialysis buffer containing citrate, and a POPC/DMPC lipid mixture, was found to be critical for obtaining large vesicles that had their entire surface packed with square arrays of AqpZ. At an optimized LPR of 0.35, micrometer large single 2D crystal sheets

were found together with vesicle-like 2D crystals, without any detectable aggregation.

AqpZ packs with $p4_212$ crystal symmetry, as does AQP1 (Walz *et al.*, 1994a), but not MIP (Hasler *et al.*, 1998b). At present, this polymorphism between molecules that share a significant sequence homology, and are similar concerning their projection structures, cannot be explained. From the mass/area value (3.19 kDa/nm²) measured by STEM on single-layered 2D crystals the LPR can be estimated, and the surface covered by the phospholipids predicted to 30%. When contouring the cryo-electron projection map of unstained 2D crystals at the steepest contrast gradient, the area covered by the lipid bilayer was found to be 31%, in excellent agreement with the STEM analysis. Mass analysis of AQP1 crystals yielded 4.1 kDa/nm² (Walz *et al.*, 1994b), explained by the additional mass of the glycosyl of about 80 kDa per unit cell.

The $p4_212$ packing arrangement allowed asymmetric negative staining to be identified (see Figure 3). Instead of merging lattice-line data from

several tilt series to produce an averaged 3D map, two different 3D reconstructions are presented, each obtained by a single tilt series recorded at low dose. These maps are strikingly different, as demonstrated by the horizontal sections in Figure 3. However, not only has the map of the deeply stained folded sheet a pronounced $p42_12$ symmetry, but it also resembles the surface topography of AqpZ crystals recorded by AFM at 7 Å resolution (Scheuring *et al.*, 1999).

Cryo-electron microscopy was performed on highly ordered 2D crystals of AqpZ, vitrified in the presence of trehalose. Adsorption of the sample to the carbon-coated copper grids and quick freezing was particularly critical, because strong interactions between the crystals and the carbon film often resulted in cracks and distortions in the crystal that could not be corrected by the standard unbending procedure. The contrast in projections of these vitrified 2D crystals is expected to result mainly from transmembrane domains rather than from flexible external loops. Closer analysis of the amino acid sequence homology between AqpZ and AQP1 reveals that the identical residues are mostly located either in the predicted six transmembrane spanning alpha-helices or in the highly conserved B and E loops that fold back into the membrane (Calamita *et al.*, 1995). Therefore, it is not surprising that the unstained projection maps of AQP1 and AqpZ display such a strong similarity (Figure 6). The similar disposition of the density maxima and minima within the tetramers suggests a helix packing arrangement in AqpZ similar to that of AQP1, which is a right-handed bundle of six tilted transmembrane alpha-helices that surround a central density (Walz *et al.*, 1997). This central density was proposed to contain the extended loops B and E (Walz *et al.*, 1997), and is also visible in the AqpZ projection map (Figure 5(b) and (c)).

Oriental cross correlation of the central AqpZ tetramer from a unit cell with that of AQP1 yielded a rotation angle of 13° (anti-clockwise) that had to be applied to the AQP1 tetramer to fit it onto the AqpZ tetramer (Figure 6(c)). Therefore, the contacts between aquaporin tetramers, which

drive the assembly of 2D crystals, may be different between AqpZ and AQP1. Comparing the projection maps of AqpZ and AQP1 tetramers after rotational alignment, correlation analysis indicated that the central tetramer of AqpZ displayed in Figure 6(d) is the view from the extracellular side as defined for AQP1 (Walz *et al.*, 1997).

The conserved structure and function of the bacterial aquaporin-Z and the human aquaporin-1 over the evolution must arise from drastic conformational and structural constraints for water specificity. The challenge now is to obtain better structural data to elucidate the mechanism providing the high water flux and specificity of these aquaporins.

Materials and Methods

Two-dimensional crystallization

Several aliquots of purified AqpZ (50 µl at 0.5 mg/ml) were incubated with a 1:1 (w/w) mixture of 1-palmitoyl-2-oleoyl-*sn*-glycero-3-phosphocholine (POPC) and 1,2-dimyristoyl-*sn*-glycero-3-phosphocholine (DMPC) (Avanti Polar Lipids, Inc. USA) at LPR values ranging from 0.3 to 2 in 2% β-octyl-glucopyranoside (OG) (Anatrace, Inc., USA). Dialysis was performed either in submerged plexi-glass wells sealed with dialysis tubing or in floating Eppendorf caps sealed with dialysis tubing. The best 2D crystals were obtained when dialysis was performed at room temperature against a 1,000× volume of 20 mM citrate (pH 6.0) buffer containing 200 mM NaCl, 100 mM MgCl₂, 3 mM NaN₃ and 10% glycerol. The dialysis buffer was changed after two days and glycerol was omitted for cryo-electron microscopy analysis. Incubation of the 2D crystals at 37°C for 12 hours was found to improve the crystal quality.

Mass/area determination in scanning transmission electron microscopy

For mass measurement, the AqpZ 2D crystals were diluted in 25 mM ammonium acetate, 150 mM NaCl (pH 7.2) and adsorbed for one minute onto glow-discharged thin carbon films that spanned a thick fenestrated carbon layer covering 200-mesh/inch, gold-plated copper grids. The grids were then blotted, washed on four drops of bi-distilled water to remove buffer salts and freeze-dried at -80°C, overnight in the microscope.

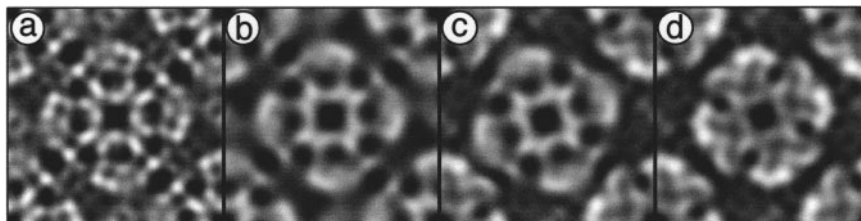


Figure 6. Comparison between AqpZ and AQP1 untitled cryo-electron projection maps at similar resolution. (a) Projection map of a single unit cell of AQP1 at 4 Å resolution, showing the central tetramer viewed from the extracellular side. (b) The same projection map of AQP1 as in (a) is rendered at a resolution of around 8 Å. (c) The central AQP1 tetramer of (b) is rotated anti-clockwise by an angle of 17° and pasted into the AqpZ projection map. (d) The AqpZ projection map at 8 Å can be compared with the AQP1 projection map (c). Similar localization of the density maxima and minima within the tetramers viewed from the extracellular side suggests a similar helix packing arrangement between AqpZ and AQP1. The sizes of the unit cells are 96 Å (AQP1) and 95 Å (AqpZ).

Dark-field images were recorded from the unstained samples at the nominal magnification of 200,000 \times (pixel size 0.8795 nm) and an accelerating voltage of 80 kV, using a Vacuum Generators STEM HB-5, which was interfaced to a modular computer system (Tietz Video and Image Processing Systems GmbH, D-8035 Gauting). The recording dose was 330(\pm 23) electrons/nm². In addition, repeated low-dose scans were recorded from some grid regions to assess beam-induced mass loss as described by Müller *et al.* (1992). The 512 \times 512 pixels digital images were evaluated using the program package IMPSYS as outlined by Müller *et al.* (1992). After correction for beam-induced mass loss, the mass values were displayed in a histogram and approximated by Gaussian curve fitting.

Transmission electron microscopy

For single particle analysis, solubilized AqpZ particles were diluted at 0.1 mg/ml in 2% OG and adsorbed for five seconds to glow-discharged carbon-coated parlodion film supported by a copper grid, washed three times in bi-distilled water and negatively stained with 0.75% uranyl formate. Images were recorded on Kodak SO-163 film at a nominal magnification of 70,000 \times and a recording dose of typically 20 electrons/Å² using a Hitachi H-8000 transmission electron microscope operated at 100 kV.

Two-dimensional crystals were negatively stained as described for single particles except that the adsorption time on the carbon film was increased to 30 seconds. Images of 2D crystals were recorded either on Kodak SO-163 film at 50,000 \times or on a slow-scan CCD camera (Tietz Video & Imaging Processing System, Gauting, Germany) at 30,000 \times nominal magnification (pixel size 4 Å). For tilt series, the automated recording protocol from the Tietz Video & Imaging Processing System was used (Dierksen *et al.*, 1992). For each tilt series 25 pictures were taken at tilt angles ranging from -60° to $+60^\circ$ in 5° steps, yielding a total dose of 150 electrons/Å².

For cryo-electron microscopy, 2D crystals of AqpZ were prepared by addition of trehalose to a final concentration of 3-10%. The crystal suspension was applied to a copper electron microscope grid coated with a flat thin carbon film. The grid was blotted with filter paper, immediately plunged into liquid ethane and transferred using a Gatan-626 cryo-holder into a Hitachi H-8000 transmission electron microscope, operated at 200 kV with a LaB₆ filament. Electron micrographs were recorded under low dose conditions (5 electrons/Å²) at a nominal magnification of 50,000 \times on Kodak SO-163 film and developed with Kodak D19 developer.

Image processing

Micrographs were digitized using a Leafscan-45 scanner (Leaf Systems, Inc., Westborough, MA). Pixel size at the specimen was 5.7 Å for single particle averaging, 4 Å for 2D crystals in negative staining and 1 Å for 2D crystals in cryo-electron microscopy.

Image analysis of negatively stained samples was performed using the SEMPER image processing system (Saxton *et al.*, 1979). For single particle averaging, 639 particles were selected by eye and a reference was first generated by selecting about 20 particles with a distinct square-like shape, aligning them translationally as well as angularly, and calculating a first average. This centered average was used for aligning the 639 particles

(Frank, 1973) and a multivariate statistical analysis (MSA) was finally performed using seven eigenvectors for classification of all the particles into 50 clusters (van Heel & Frank, 1981). Clusters were pooled according to the dendrogram to calculate the corresponding class averages.

Micrographs of AqpZ 2D crystals were selected with an optical diffractometer (Aebi *et al.*, 1973), based on the performance of the microscope and the crystal order. Averaged projection maps of negatively stained 2D crystals and 3D reconstructions were calculated using the SEMPER image processing system (Saxton *et al.*, 1979). Residual lattice disorder of negatively stained 2D crystals was eliminated by correlation averaging (Saxton & Baumeister, 1982) and averaged unit cells were finally 4-fold symmetrized. For 3D reconstruction, lattice line data from each tilt series were fitted by interpolation and backtransformed (Smith, 1981). Stacks of horizontal sections separated by a nominal distance of 3 Å were computed from the interpolated lattice lines.

For cryo-electron microscopic image analysis, well-ordered crystalline areas of 4,096 \times 4,096 pixels (pixel size 1 Å) were processed as described (Henderson *et al.*, 1986, 1990) using the MRC image-processing programs. Distortion of the 2D crystal lattice was corrected with the program CCUNBENDE. After contrast transfer function correction, Fourier components from six crystals with IQ values \leq 4 were merged by phase origin refinement. The final averaged projection map was limited to 8 Å resolution.

Acknowledgements

The work of Ms Bettina Wolpensinger who operated the STEM to record dark-field micrographs for mass determination and the expert assistance of Dr Shirley Müller are gratefully acknowledged. The authors are indebted to Dr J. Bernard Heymann for critical proof-reading of the manuscript and helpful discussion. The work was supported by the M.E. Müller Foundation of Switzerland and the Swiss National Foundation (grant no. 31-42435.94 to A.E.). P.R. thanks the French INSERM, and the Kanton Basel for post-doctoral fellowships.

References

- Abrami, L., Simon, M., Rousselet, G., Berthonaud, V., Buhler, J. & Ripoché, P. (1994). Sequence and functional expression of an amphibian water channel, FA-CHIP: a new member of the MIP family. *Biochim. Biophys. Acta*, **1192**, 147-151.
- Aebi, U., Smith, P. R., Dubochet, J., Henry, C. & Kellenberger, E. (1973). A study of the structure of the T-layer of *Bacillus brevis*. *J. Supramol. Struct.* **1**, 498-522.
- Agre, P., Smith, B. & Preston, G. (1995). ABH and Colton blood group antigens on aquaporin-1, the human red cell water channel protein. *Transfusion Clin. Biol.* **2**, 303-308.
- Baumeister, W., Barth, M., Hegerl, R., Guckenberger, R., Hahn, M. & Saxton, W. O. (1986). Three-dimensional structure of the regular surface layer (HPI layer) of *Deinococcus radiodurans*. *J. Mol. Biol.* **187**, 241-253.
- Beuron, F., Le, Cahérec F., Guillam, M.-T., Cavalier, A., Garret, A., Tassan, J.-P., Delamarche, C., Schultz, P.,

- Mallouh, V., Rolland, J.-P., Hubert, J.-F., Gouranton, J. & Thomas, D. (1995). Structural analysis of a MIP family protein from the digestive tract of *Cicadella viridis*. *J. Biol. Chem.* **270**, 17414-17422.
- Borgnia, M., Kozono, D., Calamita, G., Nielsen, S., Maloney, P. C. & Agre, P. (1999). Functional reconstitution and characterization of *E. coli* aquaporin-Z. *J. Mol. Biol.* **291**, 1169-1179.
- Calamita, G., Bishai, W., Preston, G., Guggino, W. & Agre, P. (1995). Molecular cloning and characterization of AqpZ, a water channel from *Escherichia coli*. *J. Biol. Chem.* **270**, 29063-29066.
- Calamita, G., Kempf, B., Bonhivers, M., Bishai, W. R., Bremer, E. & Agre, P. (1998). Regulation of the *Escherichia coli* water channel gene aqpZ. *Proc. Natl Acad. Sci. USA*, **95**, 3627-31.
- Cheng, A. C., vanHoek, A. N., Yeager, M., Verkman, A. S. & Mitra, A. K. (1997). Three-dimensional organization of a human water channel. *Nature*, **387**, 627-630.
- Deen, P. M. T., Verdijk, M. A. J., Knoers, N. V. A. M., Wieringa, B., Monnens, L. A. H., van Os, C. H. & van Oost, B. A. (1995). Human kidney water channel Aquaporin-2 is involved in vasopressin dependent concentration of urine. *Science*, **264**, 92-95.
- Dierksen, K., Typke, D., Hegerl, R., Koster, A. J. & Baumeister, W. (1992). Towards automatic electron tomography. *Ultramicroscopy*, **40**, 71-87.
- Finkelstein, A. (1987). *Water Movement Through Lipid Bilayers, Pores, and Plasma Membranes: Theory and Reality*, John Wiley and Sons, New York, New York.
- Frank, J. (1973). Computer processing of electron micrographs. In *Advanced Techniques in Biological Electron Microscopy* (Koehler, J., ed.), pp. 215-274, Springer-Verlag, Berlin.
- Hasler, L., Heymann, J. B., Walz, T., Kistler, J. & Engel, A. (1998a). 2D crystallization of membrane proteins: Rationales and examples. *J. Struct. Biol.* **121**, 162-171.
- Hasler, L., Walz, T., Tittmann, P., Gross, H., Kistler, J. & Engel, A. (1998b). Purified lens major intrinsic protein (MIP) forms highly ordered tetragonal two-dimensional arrays by reconstitution. *J. Mol. Biol.* **279**, 855-864.
- Henderson, R., Baldwin, J. M., Downing, K. H., Lepault, J. & Zemlin, F. (1986). Structure of purple membrane from *Halobacterium halobium*: recording, measurement and evaluation of electron micrographs at 3.5 Å resolution. *Ultramicroscopy*, **19**, 147-178.
- Henderson, R., Baldwin, J. M., Ceska, T. A., Zemlin, F., Beckmann, E. & Downing, K. H. (1990). Model for the structure of bacteriorhodopsin based on high-resolution electron cryo-microscopy. *J. Mol. Biol.* **213**, 899-929.
- Jap, B. K. & Li, H. (1995). Structure of the osmo-regulated H₂O-channel, AQP-CHIP, in projection at 3.5 Å resolution. *J. Mol. Biol.* **251**, 413-420.
- Jap, B. K., Zulauf, M., Scheybani, T., Hefti, A., Baumeister, W., Aebi, U. & Engel, A. (1992). 2D crystallization: from art to science. *Ultramicroscopy*, **46**, 45-84.
- Jung, J., Preston, G., Smith, B., Guggino, W. & Agre, P. (1994). Molecular structure of the water channel through aquaporin CHIP. The hourglass model. *J. Biol. Chem.* **269**, 14648-14654.
- King, L. S. & Agre, P. (1996). Pathophysiology of the aquaporin water channels. *Annu. Rev. Physiol.* **58**, 619-648.
- Le, Cahérec F., Deschamps, S., Delamarche, C., Pellerin, I., Bonnec, G., Guillam, M.-T., Thomas, D., Gouranton, J. & Hubert, J.-F. (1996). Molecular cloning and characterization of an insect aquaporin. Functional comparison with aquaporin 1. *Eur. J. Biochem.* **241**, 707-715.
- Li, H., Lee, S. & Jap, B. K. (1997). Molecular design of aquaporin-1 water channel as revealed by electron crystallography. *Nature Struct. Biol.* **4**, 263-265.
- Müller, D. J. & Engel, A. (1997). The height of biomolecules measured with the atomic force microscope depends on electrostatic interactions. *Biophys. J.* **73**, 1633-1644.
- Müller, S. A., Goldie, K. N., Bürki, R., Häring, R. & Engel, A. (1992). Factors influencing the precision of quantitative scanning transmission electron microscopy. *Ultramicroscopy*, **46**, 317-334.
- Park, J. H. & Saier, M. H. (1996). Phylogenetic characterization of the MIP family of transmembrane channel proteins. *J. Membr. Biol.* **153**, 171-180.
- Preston, G. M. & Agre, P. (1991). Isolation of the cDNA for erythrocyte integral membrane protein of 28 kilodaltons: member of an ancient channel family. *Proc. Natl Acad. Sci. USA*, **88**, 11110-11114.
- Saxton, W. O., Pitt, J. T. & Horner, M. (1979). The SEM-PEM image processing system. *Ultramicroscopy*, **4**, 343-354.
- Saxton, W. O. & Baumeister, W. (1982). The correlation averaging of a regularly arranged bacterial cell envelope protein. *J. Microsc.* **127**, 127-138.
- Scheuring, S., Ringler, P., Borgnia, M., Stahlberg, H., Müller, D. J., Agre, P. & Engel, A. (1999). High resolution AFM topographs of the *Escherichia coli* waterchannel aquaporin Z. *EMBO J.* in the press.
- Shiels, A. & Bassnett, S. (1996). Mutations in the founder of the MIP gene family underlie cataract development in the mouse. *Nature Genet.* **12**, 212-215.
- Smith, B. L. & Agre, P. (1991). Erythrocyte M_r 28,000 transmembrane protein exists as a multisubunit oligomer similar to channel proteins. *J. Biol. Chem.* **266**, 6407-6415.
- Smith, P. (1981). Bilinear Interpolation of Digital Images. *Ultramicroscopy*, **6**, 201-204.
- van Heel, M. & Frank, J. (1981). Use of multivariate statistics in analysing the images of biological macromolecules. *Ultramicroscopy*, **6**, 187-94.
- Verbavatz, J.-M., Brown, D., Sabolic, I., Valenti, G., Ausiello, D. A., Van Hoek, A. N., Ma, T. & Verkman, A. S. (1993). Tetrameric assembly of CHIP28 water channels in liposomes and cell membranes: a freeze-fracture study. *J. Cell Biol.* **123**, 605-618.
- Verkman, A., Shi, L., Frigeri, A., Hasegawa, H., Farinas, J., Mitra, A., Skach, W., Brown, D., Van H., A. & Ma, T. (1995). Structure and function of kidney water channels. *Kidney Int.* **48**, 1069-1081.
- Walz, T., Smith, B. L., Agre, P. & Engel, A. (1994a). The three-dimensional structure of human erythrocyte aquaporin CHIP. *EMBO J.* **13**, 2985-2993.
- Walz, T., Smith, B., Zeidel, M., Engel, A. & Agre, P. (1994b). Biologically active two-dimensional crystals of aquaporin CHIP. *J. Biol. Chem.* **269**, 1583-1586.
- Walz, T., Typke, D., Smith, B. L., Agre, P. & Engel, A. (1995). Projection map of aquaporin-1 determined by electron crystallography. *Nature Struct. Biol.* **2**, 730-732.

- Walz, T., Hirai, T., Murata, K., Heymann, J. B., Mitsuoka, K., Fujiyoshi, Y., Smith, B. L., Agre, P. & Engel, A. (1997). The 6 Å three-dimensional structure of aquaporin-1. *Nature*, **387**, 624-627.
- Weig, A., Deswarte, C. & Chrispeels, M. J. (1997). The major intrinsic protein family of *Arabidopsis* has 23 members that form three distinct groups with functional aquaporins in each group. *Pl. Physiol.* **114**, 1347-1357.
- Zampighi, G., Simon, S. A., Robertson, J. D., McIntosh, T. J. & Costello, M. J. (1982). On the structural organization of isolated bovine lens fiber junctions. *J. Cell Biol.* **93**, 175-189.

Edited by W. Baumeister

(Received 22 March 1999; received in revised form 21 June 1999; accepted 2 July 1999)